

Incorporating numerical modeling into estimates of the detection capability of the IMS infrasound network

A. Le Pichon,¹ L. Ceranna,² and J. Vergoz¹

Received 2 August 2011; revised 17 January 2012; accepted 17 January 2012; published 9 March 2012.

[1] To monitor compliance with the Comprehensive Nuclear-Test ban Treaty (CTBT), a dedicated International Monitoring System (IMS) is being deployed. Recent global scale observations recorded by this network confirm that its detection capability is highly variable in space and time. Previous studies estimated the radiated source energy from remote observations using empirical yield-scaling relations which account for the along-path stratospheric winds. Although the empirical wind correction reduces the variance in the explosive energy versus pressure relationship, strong variability remains in the yield estimate. Today, numerical modeling techniques provide a basis to better understand the role of different factors describing the source and the atmosphere that influence propagation predictions. In this study, the effects of the source frequency and the stratospheric wind speed are simulated. In order to characterize fine-scale atmospheric structures which are excluded from the current atmospheric specifications, model predictions are further enhanced by the addition of perturbation terms. A theoretical attenuation relation is thus developed from massive numerical simulations using the Parabolic Equation method. Compared with previous studies, our approach provides a more realistic physical description of long-range infrasound propagation. We obtain a new relation combining a near-field and a far-field term, which account for the effects of both geometrical spreading and absorption. In the context of the future verification of the CTBT, the derived attenuation relation quantifies the spatial and temporal variability of the IMS infrasound network performance in higher resolution, and will be helpful for the design and prioritizing maintenance of any arbitrary infrasound monitoring network.

Citation: Le Pichon, A., L. Ceranna, and J. Vergoz (2012), Incorporating numerical modeling into estimates of the detection capability of the IMS infrasound network, *J. Geophys. Res.*, *117*, D05121, doi:10.1029/2011JD016670.

1. Introduction

[2] Interest in infrasound technology and research was revived after the Comprehensive Nuclear-Test ban Treaty (CTBT) was adopted and opened for signature in 1996. The renaissance in infrasound research is currently stimulated by the development of a global 60-station network of microbarometer arrays as one of the verification measures for the CTBT. This International Monitoring System (IMS) infrasound network is designed to detect and locate explosions with a yield of one kiloton of TNT anywhere in the world with at least two stations [e.g., *Christie et al.*, 2001; *Christie and Campus*, 2010]. Even though the IMS infrasound network is not yet fully established, its data have been exploited in numerous source, propagation and detection studies [e.g., *Campus and Christie*, 2010; *Brachet et al.*, 2010].

[3] Global scale studies have highlighted factors affecting the performance of the network, including the influence of upper atmospheric winds from hourly to seasonal timescales, station noise and source frequency [*Garcés et al.*, 1998; *Drob et al.*, 2003; *Le Pichon et al.*, 2009; *Green and Bowers*, 2010]. Depending on the atmospheric wind structure, infrasonic waves may propagate in acoustic waveguides between the ground and troposphere, stratosphere and lower thermosphere [*Brown et al.*, 2002; *Drob et al.*, 2003]. Multiple arrivals, referred to as phases, may then be recorded at the receiver. They correspond to a specific family of raypaths and turning-height levels in the atmosphere, and are characterized by specific values of frequency, amplitude, incidence angle and direction of arrival.

[4] In order to model the detection capability of an infrasound network, it is necessary to predict the signal amplitude at any location, and further evaluate whether the signal is detectable above the noise level at the receivers. Different approaches incorporating background noise and various yield-scaling relationships have been proposed [e.g., *Sereno et al.*, 1990; *Barker*, 1996; *Clauter and Blandford*, 1997; *Trost*, 1997]. Significant advances were achieved by *Stevens et al.* [2002] by considering attenuation relations derived from

¹CEA/DAM/DIF, Arpajon, France.

²BGR, Hannover, Germany.

recordings of historical atmospheric nuclear and chemical explosions [e.g., *Whitaker*, 1995]. However, conclusions from these studies may be misleading because they do not include an accurate description of the time varying stratospheric winds and where limited to stratospheric arrivals from relatively low yield explosions.

[5] One dominant factor influencing infrasound detection is the seasonal oscillation of the dominant east-west (zonal) component of the stratospheric wind flow [e.g., *Balachandran et al.*, 1971]. This oscillation, clearly captured in climatological wind models [e.g., *Drob et al.*, 2003], controls to first order where infrasound signals are expected to be detected since detection capability is preferable downwind [e.g., *Whitaker and Mutschlecner*, 2008]. Using state-of-the-art specifications of the stratospheric winds and time-dependent station noise models, recent simulations predicted that explosions equivalent to ~ 500 t of TNT would be detected by at least two stations at any time of the year over the earth's surface [*Le Pichon et al.*, 2009]. More recently, *Green and Bowers* [2010] extended the probabilistic approach of *Clauter and Blandford* [1997] and *Stevens et al.* [2002] for predicting the minimum yield required to ensure 90% probability of detection at two or more stations. When accounting for low station noise at frequencies above 0.2 Hz, simulations predict that explosions equivalent to ~ 200 t of chemical explosive would be detected over $\geq 95\%$ of the earth's surface at any time of the year. These results are consistent with average detection thresholds published by *Le Pichon et al.* [2009].

[6] However, these previous studies simplified the complexities of infrasound propagation using an empirical yield-amplitude scaling relation [e.g., *Whitaker et al.*, 2003]. The following Los Alamos National Laboratory (LANL) relation was established from a comprehensive data set including infrasound signals propagating to ranges of up to a few hundred kilometers [*Whitaker*, 1995],

$$\log P = 1.33 + 0.68 \times \log E - 1.36 \times \log R + 0.019 V_s \quad (1)$$

where P is the zero-to-peak pressure amplitude (in Pa), E is the yield (in tons of TNT equivalent), R is the source-to-receiver distance (in km), and V_s is the stratospheric wind speed averaged along the raypath at 50 km altitude (in m/s). Although *Stevens et al.* [2002] demonstrated that the LANL relation provided the best agreement with data from historic nuclear tests carried out at the Nevada Test Site, equation (1) does not adequately describe infrasound propagation nor make full use of available high-resolution atmospheric models. A first limitation is the use of one single wind correction parameter over the propagation path. By analyzing well-calibrated reference events, erroneous attenuation estimates were found due to either large variability in along-path wind speed in the stratosphere [*Ceranna et al.*, 2009; *Green et al.*, 2011], or a systematic over-estimate of a known yield [*Gitterman et al.*, 2009]. A second limitation is that the relation is essentially applicable to stratospheric returns and high-frequency signals generated by low yield explosions. Although most of the detected signals in the frequency band of interest propagate in a stratospheric waveguide, thermospheric arrivals may be recorded upwind of the source. Models predicting attenuation relations of all observed arrivals, such as those proposed by *Whitaker*

and *Mutschlecner* [2008] would provide more realistic detection levels for local tropospheric ducts and long propagation range scenarios for stratospheric and thermospheric arrivals.

[7] Modeling techniques coupled with realistic atmospheric specifications are widely used to improve propagation predictions [e.g., *Norris et al.*, 2010]. The high-frequency wave approximation implicit in ray-tracing models is inappropriate for such studies, as the ray-theory derived amplitude fails to deal with wavefront folding phenomena in an inhomogeneous medium and the formation of caustics [*Blom and Waxler*, 2010]. Frequency domain numerical methods that include the effects of both wind and attenuation are needed. Here, realistic simulations are achieved using a linear wide-angle Parabolic Equation (PE) method as an effective technique for propagating acoustic energy in a stratified atmosphere [*Lingevitch et al.* 2002].

[8] Although global atmospheric models can resolve wind velocity variations on short timescales [e.g., *Kulichkov and Bush*, 2001], difficulties in interpreting infrasound signals arise due to uncertainties in the wind structure at stratospheric and mesospheric altitudes (between 35 and 80 km) [*Le Pichon et al.*, 2005; *Drob et al.*, 2010; *Green et al.*, 2011]. With the expansion of the IMS network and the growing number of experimental infrasound arrays being deployed worldwide, large reference event databases provide a key motivation for understanding how meteorological variations affect the observed arrivals [e.g., *Evers et al.*, 2007; *Ceranna et al.*, 2009; *Gainville et al.*, 2010]. Small-scale meteorological variations which are not resolved by the current atmospheric specifications affect the extent of the predicted ensonified regions and shadow zones at ground level. These effects are especially relevant in the stratosphere and lower thermosphere where gravity wave amplitudes and scale lengths are large [e.g., *Gardner et al.*, 1993; *Fritts and Alexander*, 2003]. Atmospheric gravity waves have been proposed as one potential source of the observed waveform variability over short timescales, and provide a mechanism for acoustic penetration into geometrical shadow zones [e.g., *Kulichkov et al.*, 2002]. In order to characterize the effects of fine-scale atmospheric structures, our PE simulations incorporate wind perturbation terms to the atmospheric profiles which may reach 10–20 m/s at 50 km altitude [e.g., *Green et al.*, 2011]. Improved frequency-dependent attenuation relations are derived from massive numerical simulations. To our knowledge, such a relation based on a numerical modeling approach has not been used within previous network performance predictions.

[9] In section 2, we describe the methodology employed to develop the attenuation relation. The influence of the parameters describing the source and the atmosphere on the predicted attenuation is discussed. In section 3, we present examples of detection capability simulations of the IMS infrasound network, focusing on the related effects of the stratospheric wind parameterization and source frequency on the propagation. The geographical coverage of the thresholds and their temporal fluctuations over time scales ranging from days to season are quantified. In the last section, we address the implications of our results which, compared to previous studies, provide progress toward more accurate space-, time- and frequency-dependent detection levels. Limitations of the present models are discussed along with

future developments needed to calculate detection thresholds in tons of TNT equivalent.

2. Toward an Attenuation Relation Based on Numerical Modeling

[10] We use the linear wide-angle PE method to investigate a large range of realistic propagation conditions in the frequency band of interest for detecting explosions. This technique accounts for diffraction effects near shadow zone boundaries and scattering by small atmospheric inhomogeneities and overcomes several of ray method limitations that include validity of high-frequency approximation. It implements the split-step Pade numerical scheme allowing large range and depth grid spacing [Collins, 1993]. It has been used extensively to provide reasonable accuracy in the attenuation over long propagation distances [Gibson *et al.*, 2009; Gainville *et al.*, 2010; Green *et al.*, 2011]. The chosen absorption model includes contributions from both classical (translation and diffusion) and relaxation (rotation and vibration) losses. It computes frequency-dependent attenuation coefficients from vertical profiles of temperature, pressure, and concentration of gases up to 160 km altitude [Sutherland and Bass, 2004]. These input variables are obtained from the MSISE model [Picone *et al.*, 1997]. In the presented simulations, for sake of simplicity and in order to limit the use of computational resources, the propagation problem is simplified in Cartesian coordinates assuming a planar terrain with infinite impedance at the sea level. The wind convection is included using a range-independent effective sound speed calculated in the direction of propagation. Considering the simplifying hypotheses detailed above, the model used has known limitations (e.g., numerical sensitivity near turning points and near caustics, out of plane scattering effects not included) which may introduce biases in our simulations.

[11] A reduced number of parameters describing the source and the propagation medium with significant impact on infrasound propagation has been identified and is outlined below:

[12] 1. To ensure that sufficient bands will capture signals across a wide range of source yields, two-octave overlapping frequency bands are considered [Green and Bowers, 2010]. Six bandwidths overlapping by one octave between 0.04 and 5.12 Hz are used for the simulations: 0.04 to 0.16 Hz, 0.08 to 0.32 Hz, 0.16 to 0.64 Hz, 0.32 to 1.28 Hz, 0.64 to 2.56 Hz and 1.28 to 5.12 Hz. PE simulations are carried out at the following central frequencies: 0.1, 0.2, 0.4, 0.8, 1.6, and 3.2 Hz.

[13] 2. The effective sound speed represents the combined effects of refraction due to sound speed gradients and advection due to along-path wind on infrasound propagation [e.g., Green *et al.*, 2011]. Synthetic vertical profiles are constructed by adding Gaussian correction factors on winds centered at 50 km with a half-width of 30 km, to the U.S. Standard Atmosphere [U.S. Committee on Extension to the Standard Atmosphere, 1976] temperature profile. In this study, we use the $V_{\text{eff-ratio}}$ dimensionless parameter defined by the ratio between the effective sound speed at 50 km altitude and the sound speed at the ground level. In order to cover realistic down- and counter-wind scenarios in the

stratosphere, 38 values of $V_{\text{eff-ratio}}$ ranging from 0.85 to 1.2 are considered for the simulations.

[14] 3. Since wind perturbations play an important role in returning acoustic energy to the ground [Gibson *et al.*, 2009; Kulichkov *et al.*, 2010; Norris *et al.*, 2010], horizontal velocity fluctuations of realistic amplitude induced by naturally occurring gravity waves are incorporated in the original wind models [Gardner *et al.*, 1993]. Figure 1 compares the PE attenuation for a source frequency of 0.4 and 1.6 Hz for both gravity wave and non-gravity wave simulations. When incorporating gravity waves, the acoustic penetration into the shadow zone and between the first stratospheric bounces is clearly visible. The effect is more pronounced at higher frequencies when the signal wavelengths are smaller than those of atmospheric property variations. Beyond the first stratospheric bounce, a ~ 50 dB decrease of the attenuation is noted upwind of the source when incorporating gravity waves. Also, diffracted energy is observed for $V_{\text{eff-ratio}}$ lower than one. In this study, the perturbation terms are obtained by computing 40 different realizations of spectral model of wind inhomogeneities for each effective sound speed profile [e.g., Green *et al.*, 2011; Matoza *et al.*, 2011].

[15] The effects of other parameters like the height of the maximum stratospheric wind speed (from 35 to 65 km) and the source altitude (from 0 to 30 km) have also been investigated. Few hundreds kilometers from the source, recent work has shown that elevating a source can significantly change the amount of refracted energy [Matoza *et al.*, 2011]. However, at large distances (beyond ~ 1000 km), PE simulation results have shown weaker effects on the attenuation. Considering all possible combinations of the selected input parameters, 9,120 PE simulations were performed with a source located on the earth's surface. From this synthetic data set, we propose the following attenuation formula which explains in one order of magnitude the simulation results,

$$A_P(f, V_{\text{eff-ratio}}) = \frac{1}{R} 10^{\frac{\alpha(f)R}{20}} + \frac{R^{\beta(f, V_{\text{eff-ratio}})}}{1 + 10^{\frac{\delta-R}{\sigma(f)}}} \quad (2)$$

where A_p is the attenuation coefficient of the pressure wave at a distance R (in km) from the source. The attenuation is calculated from the source region at a reference distance of 1 km to the receiver. We assume that above this reference distance, infrasound can be treated as linear elastic waves rather than nonlinear shock waves.

[16] Equation (2) consists of a near-field and far-field term, and four parameters α , β , δ , and σ . The near-field term describes the attenuation in the shadow zone by spherical geometrical spreading combined with an exponential decay where α (in km^{-1}) is the dissipation of direct waves [e.g., Beranek, 1954]. The far-field term describes the attenuation in the geometrical acoustic duct region. Here, the attenuation is controlled by three parameters: β which accounts for the geometrical spreading and dissipation of stratospheric and thermospheric waves, δ (in km) which defines the width of the shadow zone, and σ (in km) which is a scaling distance controlling the strength of the attenuation in the shadow zone.

[17] The four parameters α , β , δ , and σ are calculated using a multidimensional curve-fitting approach. Tables 1a, 1b, and 1c provide the mean values of (α , β , σ) by applying a

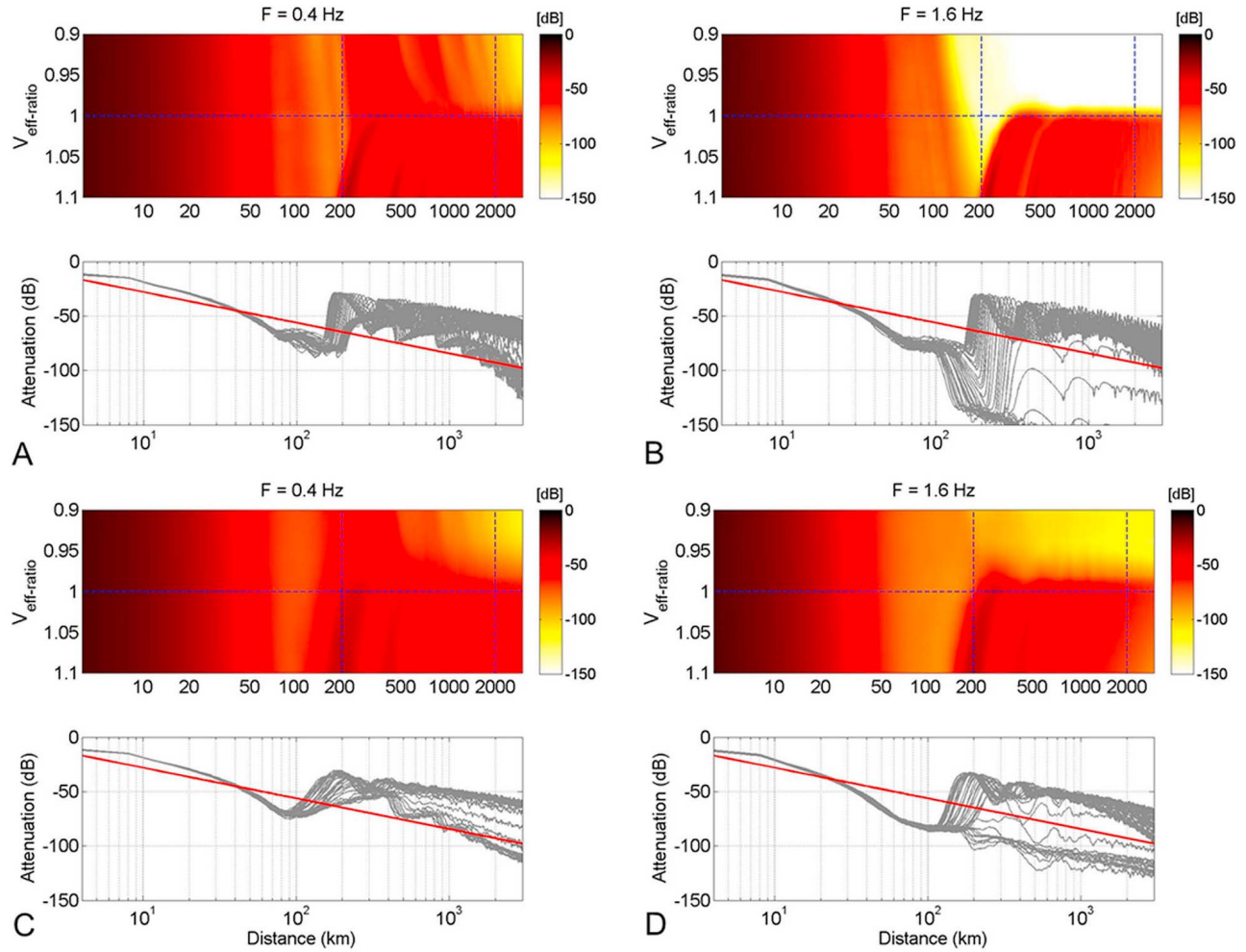


Figure 1. Comparison between PE simulations for a source frequency of (a and c) 0.4 Hz and (b and d) 1.6 Hz. Simulations are performed with (Figures 1c and 1d) and without (Figures 1a and 1b) including gravity waves. In each pair of panels, the upper panel shows the 2-D attenuation versus distance and $V_{\text{eff-ratio}}$. The color scale codes the pressure attenuation (in dB) calculated from the source at a reference distance of 1 km to the receiver located at the ground level, 2 to 3000 km away from the source. The horizontal dashed line corresponds to $V_{\text{eff-ratio}} = 1$. The vertical dashed lines at 200 and 2000 km approximately indicate the first stratospheric bounce (edge of the shadow zone). In each pair of panels, the lower graphs show the 1-D attenuation versus range for various values of $V_{\text{eff-ratio}}$ (gray lines). The red line indicates the attenuation derived from the empirical LANL relation (equation (1)) when $V_{\text{eff-ratio}} = 1$.

nonlinear least squares algorithm to the synthetic simulation data set [More, 1977]. Although not strictly correct, δ is here assumed to be constant. The corresponding uncertainties of these parameters are derived from the standard deviations of multiple gravity wave realizations. Figure 2 compares the predicted pressure attenuation to the curve-fitting results for different source frequencies as a function of $V_{\text{eff-ratio}}$. The proposed theoretical attenuation relation explains the main expected features of the propagation in the classical shadow zone and the geometrical acoustic duct region.

[18] At ranges below ~ 200 km, the attenuation weakly depends on stratospheric wind conditions, since near the source few rays reach stratospheric altitudes. The transmission loss in the shadow zone α increases with frequency (from $-0.28 \pm 0.05 \text{ km}^{-1}$ at 0.1 Hz to -0.69 ± 0.06 at 3.2 Hz).

[19] PE simulations predict that the width of the shadow zone δ between the source and the first stratospheric bounce decreases with increasing wind speed (from ~ 250 km for $V_{\text{eff-ratio}}$ slightly lower than 1 down to ~ 150 km for

Table 1a. Mean and Standard Deviation of the Parameter α (km^{-1}) Depending on the Source Frequency and the Effective Sound Speed Ratio Ranging From 0.85 to 1.18

f (Hz)	Mean	STD
0.1	-0.28	0.05
0.2	-0.33	0.04
0.4	-0.39	0.03
0.8	-0.47	0.04
1.6	-0.59	0.06
3.2	-0.69	0.06

Table 1b. Mean and Standard Deviation of the Parameter β (km^{-1}) Depending on the Source Frequency and the Effective Sound Speed Ratio Ranging From 0.85 to 1.18

f (Hz)	$V_{\text{eff-ratio}}$																			
	0.85	0.88	0.91	0.94	0.97	1.0	1.03	1.06	1.09	1.12	1.15	1.18								
0.1	Mean	STD	Mean	STD	Mean	STD	Mean	STD	Mean	STD	Mean	STD	Mean	STD						
0.1	-1.00	0.10	-1.00	0.10	-1.00	0.10	-1.00	0.10	-0.90	0.05	-0.85	0.10	-0.85	0.10	-0.85	0.10	-0.80	0.10	-0.80	0.05
0.2	-1.20	0.10	-1.20	0.10	-1.15	0.10	-1.10	0.10	-1.05	0.10	-0.95	0.10	-0.90	0.10	-0.85	0.10	-0.85	0.10	-0.85	0.10
0.4	-1.35	0.15	-1.40	0.15	-1.40	0.15	-1.35	0.15	-1.15	0.15	-1.00	0.10	-0.90	0.10	-0.90	0.10	-0.85	0.10	-0.85	0.10
0.8	-1.70	0.15	-1.60	0.20	-1.60	0.15	-1.55	0.20	-1.30	0.15	-1.05	0.15	-0.90	0.10	-0.90	0.10	-0.90	0.10	-0.90	0.10
1.6	-1.95	0.30	-1.95	0.25	-1.85	0.20	-1.75	0.25	-1.40	0.20	-1.15	0.20	-0.95	0.10	-0.95	0.10	-1.00	0.10	-1.00	0.10
3.2	-2.40	0.45	-2.30	0.30	-2.10	0.25	-1.85	0.25	-1.45	0.25	-1.20	0.20	-1.00	0.10	-1.00	0.10	-1.05	0.10	-1.10	0.10

$V_{\text{eff-ratio}} = 1.18$) as stronger along-path wind reduces ray turning height (Figure 2). However, we consider this range of variation of second order effect for global performance studies. In this study, δ is wind- and frequency-independent and set to 180 ± 50 km.

[20] The ensonification of the shadow zone is essentially driven by the frequency. Tropospheric ducts may also propagate energy in the shadow zone. However, they are not considered in this study. This is indicated by the scaling distance σ which controls the maximum attenuation in the shadow zone. It increases when transmission losses decrease with frequency. Between 0.1 and 3.2 Hz, σ decreases from 79 ± 22 km down to 20 ± 3 km.

[21] Beyond the shadow zone, the frequency and $V_{\text{eff-ratio}}$ control to a first order the pressure attenuation. The transmission loss β in the geometric acoustic duct region combines the effects of both geometrical spreading and dissipation on the wave amplitude. In case of downwind propagation ($V_{\text{eff-ratio}} > 1$), sound refracted in the stratosphere returns to the ground and propagates with weak attenuation. The attenuation parameter β is roughly constant in the studied frequency range ($\beta = -0.92 \pm 0.05$). This behavior is in contrast to propagation occurring in upwind direction ($V_{\text{eff-ratio}} < 1$). At 0.1 Hz, the attenuation is almost comparable to downwind propagation condition with β in the order of -1 . Above 0.8 Hz, sound propagating upwards is attenuated due to the low particle density and nonlinear dissipation in the thermosphere [Sutherland and Bass, 2004]. Between 0.8 and 3.2 Hz, a much stronger attenuation is predicted with $\beta = -1.78 \pm 0.12$. For $V_{\text{eff-ratio}}$ slightly lower than one, where ray tracing techniques would fail to predict stratospheric returns, the PE simulations incorporating gravity waves enlarge the ensonified regions at ground level. This is clearly reflected in Table 1b where the standard deviation of β increases with frequency as gravity wave perturbations control the appearance of the stratospheric duct; for $V_{\text{eff-ratio}}$ ranging from 0.97 to 1.03, the relative standard deviation of β increases from $\sim 10\%$ at 0.1 Hz to $\sim 20\%$ at 3.2 Hz.

[22] According to the PE modeling, the stratospheric duct starts refracting acoustic energy back to the ground for $V_{\text{eff-ratio}}$ larger than one, hence decreasing the transmission loss. Simulations also show that at large distance from the source (beyond ~ 1000 km), a further increase in the wind speed will not significantly influence the amount of returned energy. This effect is in contradiction with the empirical wind term incorporated in equation (1) which predicts an exponential decrease of the attenuation with increasing wind speed.

[23] Any significant wind component in the stratosphere such that $V_{\text{eff-ratio}} > 1$ will generate signals of approximately the same amplitude. This is consistent with the theoretical work of Kulichkov [2010] regarding partial and total reflections. In the work of Kulichkov [2010], infrasound signals from a series of repeating explosions with energy equivalent to 20–70 tons of TNT were systematically analyzed. They showed that the pulsed component of the observed signals is formed by infrasonic wave features at turning heights where $V_{\text{eff-ratio}} > 1$. Thus, the time variations of the observed signals are essentially caused by changes in the structure of $V_{\text{eff-ratio}}$ rather than the stratospheric wind strength only.

[24] Figure 3 compares the attenuation curves using equation (2) for a source frequency of 0.1, 0.2, 0.4, 0.8, 1.6, and 3.2 Hz, and an effective sound speed ratio ranging from 0.85 to 1.18. It highlights the attenuation above 200 km. As discussed above, the attenuation in the shadow zone does not depend on $V_{\text{eff-ratio}}$. Between 0.1 and 3.2 Hz, the transmission loss increases by ~ 50 dB. For horizontal propagation ranges larger than ~ 200 km, while the attenuation is roughly constant when $V_{\text{eff-ratio}} > 1$, the attenuation strongly increases with frequency when upwind propagation occurs. At a distance of 1000 km from the source, the attenuation increases by ~ 80 dB from 0.1 to 3.2 Hz.

[25] Equation (2) differs from previous empirical formulations normalizing signals for atmospheric effects. The main difference between equation (1) and equation (2) is the effect of the stratospheric winds on attenuation. The 0.019 V_s factor in equation (1) predicts a smooth variation in signal amplitude with changing wind speed. On the contrary, the PE modeling accounts for an approximately binary variation of the attenuation for $V_{\text{eff-ratio}}$ below and above 1. This feature is consistent with most multiyear global infrasound observations that indicate good detection capability for downwind stations even when $V_{\text{eff-ratio}}$ is only slightly above

Table 1c. Mean and Standard Deviation of the Parameter σ (km) Depending on the Source Frequency and the Effective Sound Speed Ratio Ranging From 0.85 to 1.18

f (Hz)	Mean	STD
0.1	79	22
0.2	55	10
0.4	43	4
0.8	36	4
1.6	27	7
3.2	20	3

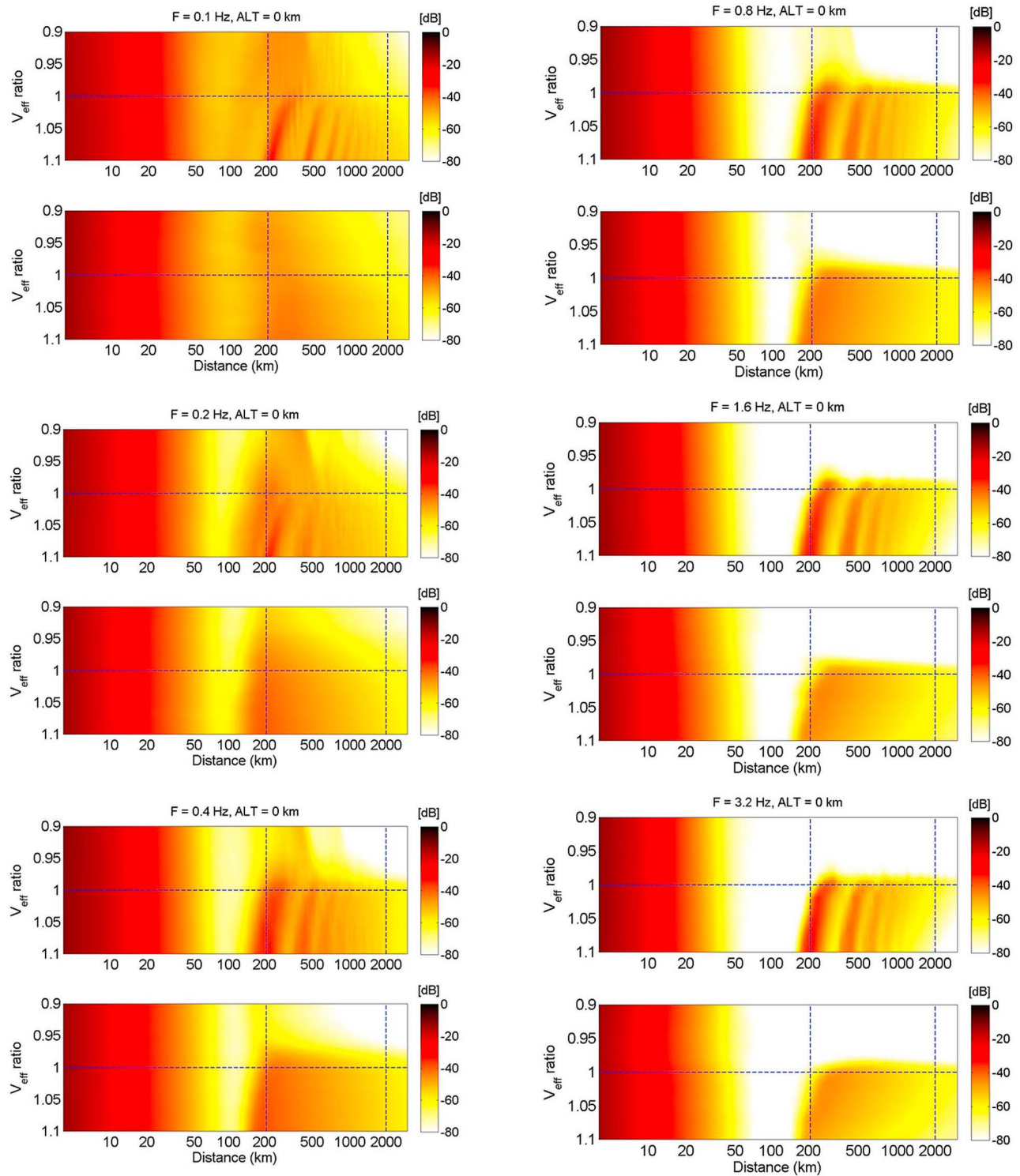


Figure 2. Comparison between PE simulations for a source frequency of 0.1, 0.2, 0.4, 0.8, 1.6, and 3.2 Hz and the multidimensional curve-fitting results. For each frequency, the top and bottom panels present the simulation and multidimensional curve-fitting results, respectively. The color scale codes the pressure attenuation (in dB) calculated from the source at a reference distance of 1 km to the receiver.

1 [Le Pichon et al., 2010]. One reason for this difference may be caused by the fact that most LANL stations showing the most striking variability with stratospheric wind speed were positioned in a range of ~ 250 km from the source.

As shown by Figure 2, a station located within such a range is expected to exhibit large amplitude variations when $V_{\text{eff-ratio}} \sim 1$. As the size of the shadow zone reduces with increasing wind speed, a station at 150–200 km from the

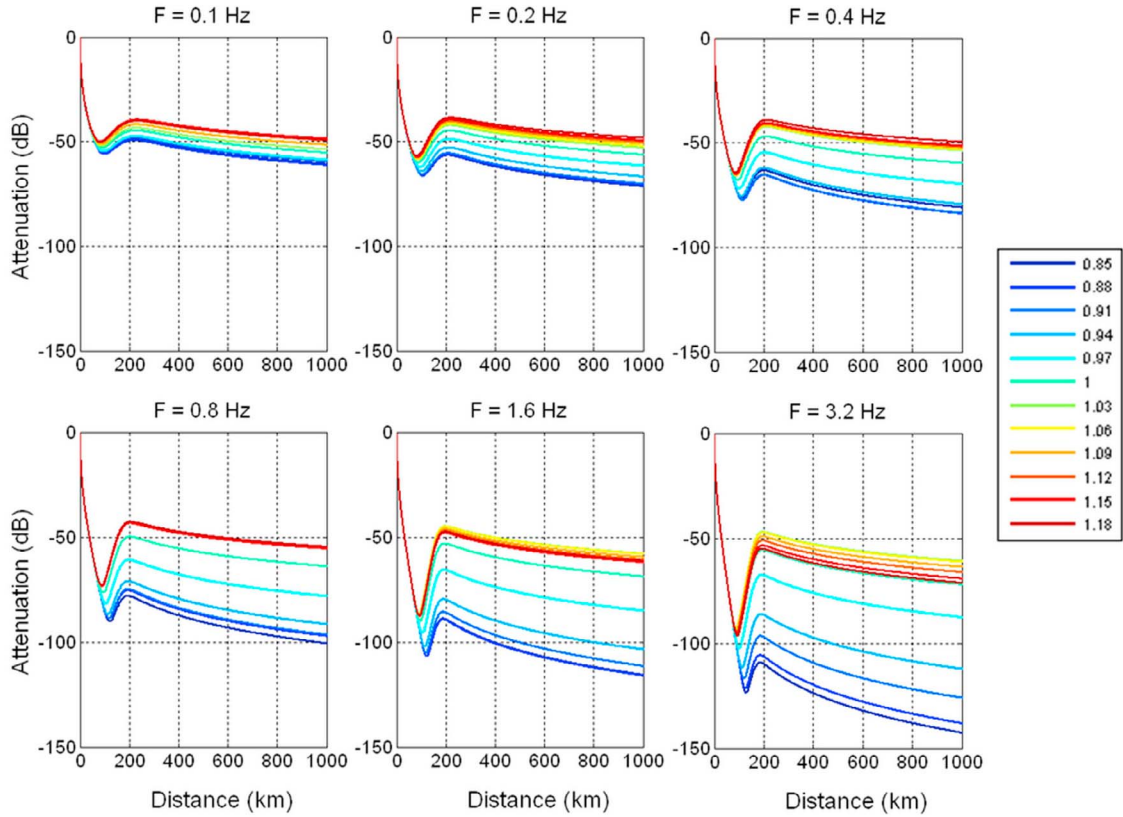


Figure 3. Attenuation curves versus distance using the multidimensional curve fitting relation at frequencies of 0.1, 0.2, 0.4, 0.8, 1.6, and 3.2 Hz. The color refers to the effective sound speed ratio ranging from 0.85 to 1.18.

source may move into the geometrical acoustic duct region considered to be a homogeneous waveguide.

3. Application to the Global IMS Infrasound Network

[26] To evaluate the performance of the IMS network, we consider the constraints on calculating the smallest signal attenuation at all stations. From equation (2), we compute $A_P[k, f](i, j)$, where k ($1 \leq k \leq M$) is the index of M stations sorted with respect to the attenuation coefficient (from lowest to highest values), f is the source frequency ($f = 0.1, 0.2, 0.4, 0.8, 1.6, \text{ and } 3.2$ Hz), and (i, j) is the source grid in latitude and longitude covering the globe. Further developments that are out of the scope of this study are needed to derive the minimum detectable signals amplitude from the smallest signal attenuation. Assuming a background noise (N) and a minimum signal-to-noise ratio (SNR) at which a detection can be confidently made, the minimum detectable signal amplitude at a frequency (f) and at point (i, j) with respect to station (k) will be given by

$$\frac{N(k, f) \cdot \text{SNR}(k)}{A_P[k, f](i, j)} \quad (3)$$

The stratospheric wind V_s used in the simulations is derived from the European Center for Medium range Weather Forecasting (ECMWF, <http://www.ecmwf.int>) models. The

latter model provides improved parameterization of the atmospheric vertical structure within the stratospheric region of interest. For one specific date and time, the stratospheric wind term $\bar{V}_s[k](i, j)$ is averaged at 50 km altitude along the great circle arc between each node (i, j) of the source grid and each array (k). Then, the corresponding value for $\bar{V}_{eff-ratio}[k](i, j)$ is given by the ratio between $\bar{V}_s[k](i, j)$ and the sound speed $\bar{C}_{z=0}[k](i, j)$ at the ground level. Finally, the smallest signal attenuation $A_P[k, f](i, j)$ is calculated given f and $\bar{V}_{eff-ratio}[k](i, j)$ following a two-dimensional cubic interpolation of the matrices (α, β, σ) presented in Tables 1a, 1b, and 1c. Using equation (2), the performance of the full IMS network is calculated using a $1^\circ \times 1^\circ$ global source grid. We also investigate the effect of the number of detecting stations on the network performance with one-, two- and three-station coverage. These calculations are run at 0.1, 0.2, 0.4, 0.8, 1.6, and 3.2 Hz, each day of the year. In order to explore all these scenarios, overall 13,140 global simulations have been carried out.

[27] Figure 4 compares the geographical coverage of the minimum signal attenuation at one station ($k = 1$) for different source frequencies on January 1, 2010. It highlights the dominant effects of both stratospheric wind dynamics and source frequency on the network performance. During winter, in the northern hemisphere, the steady eastward stratospheric currents favor long-range propagation of signals from westerly directions, as seen from blue regions west

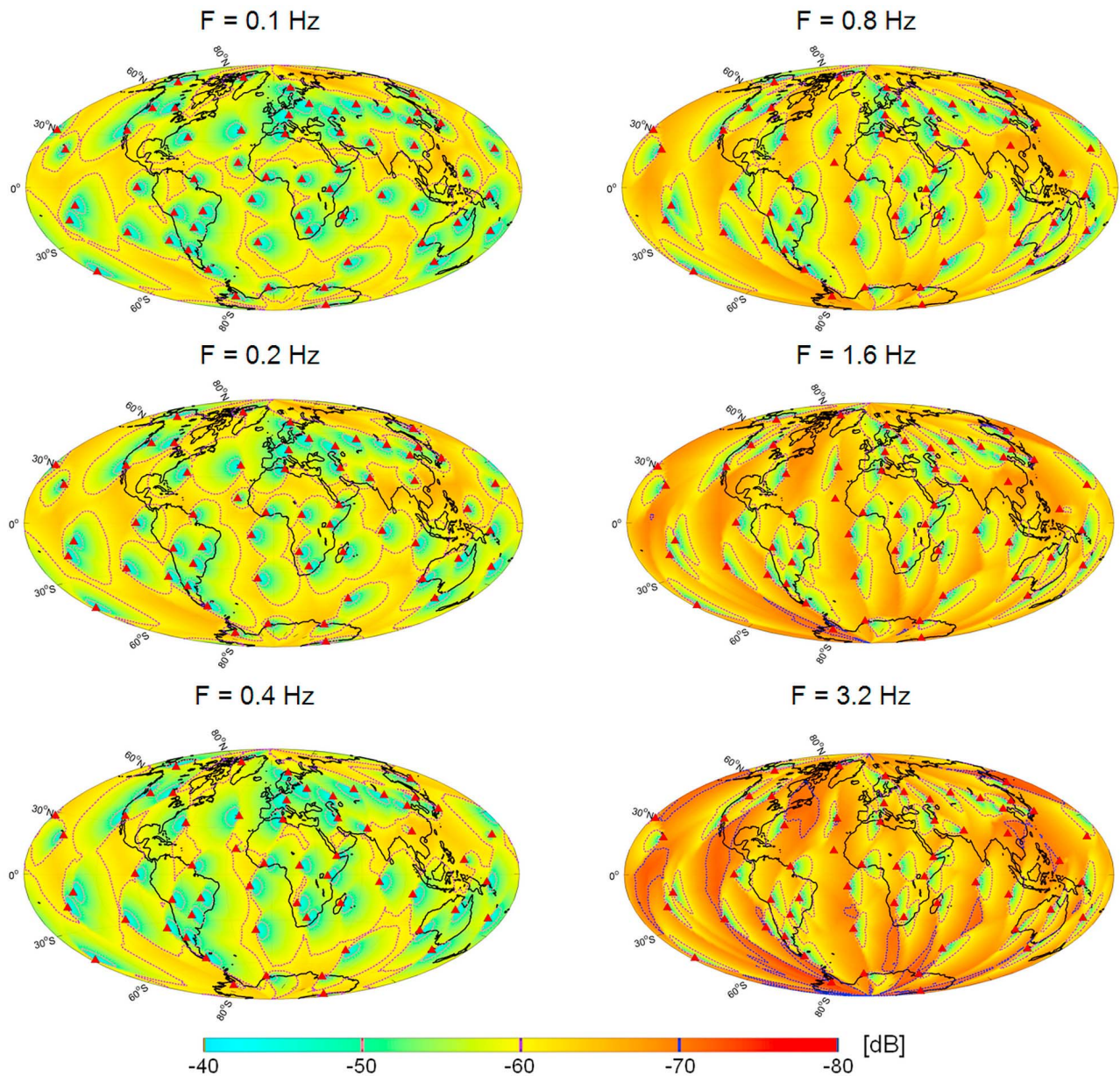


Figure 4. Geographical distribution of the smallest signal attenuation on January 1, 2010 with one-station coverage. The stratospheric wind components are derived from the ECMWF model. The red triangles indicate the location of the 59 IMS infrasound stations used for this study. The color map codes the attenuation (in dB) for sources located worldwide. Simulations are carried out at frequencies of 0.1, 0.2, 0.4, 0.8, 1.6, and 3.2 Hz.

of the stations indicating lower attenuation. In the southern hemisphere, it is the opposite as simulations predict weaker attenuation along the prevailing westward winds for sources located east of the stations. A stronger attenuation is globally noted above 0.8 Hz as well as a more pronounced directivity along the prevailing wind direction.

[28] Figure 5 compares the geographical coverage of the minimum signal attenuation for different frequencies and different seasons. As the IMS infrasound network was designed to detect and locate atmospheric explosions, two-station coverage ($k = 2$) is considered as the baseline condition to form an event. Improved performance is predicted during the solstice

periods (January and July) when the stratospheric winds are the strongest, compared to the equinox periods (April and October) when zonal winds reduce and reverse. Such effects have already been pointed out by *Le Pichon et al.* [2009] and *Green and Bowers* [2010]. The largest seasonal variations of the attenuation are observed in the equatorial regions where weak stratospheric winds yield a general increase of the attenuation. It is noteworthy that even under low wind conditions, favorable propagation conditions remain over extended midlatitude regions in both hemispheres.

[29] Figure 6 presents the yearly fluctuations of the smallest signal attenuation with one-, two- and three-station

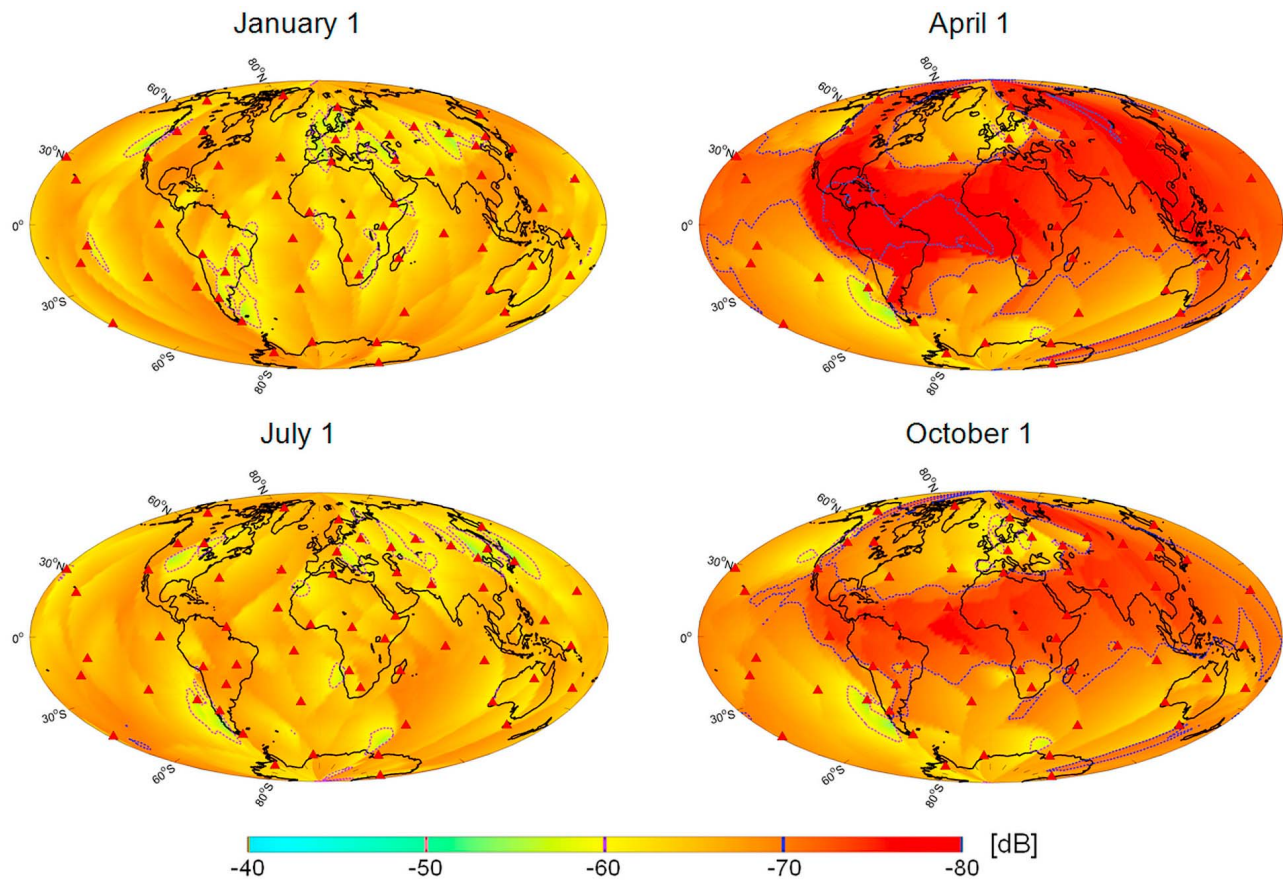


Figure 5. Geographical distribution of the smallest signal attenuation on January 1, April 1, July 1 and October 1, 2010 with two-station coverage. The stratospheric wind components are derived from the ECMWF model. Simulations are carried out at a frequency of 0.8 Hz.

coverage (corresponding to an average inter-station spacing of ~ 2000 , 2290 and 2520 km, respectively). Compared with two-station coverage, three stations offer the advantage of reduced false alarms through redundant station detections, and improved location accuracy through reduction of sites aligned with the source. As expected, the network performance follows the general stratospheric wind circulation. A significant performance enhancement is predicted in winter and summer when the prevailing stratospheric jet currents favor long-range propagation. During the transition between winter and summer, zonal winds reduce and reverse, yielding higher attenuation. Previous detection capability studies have shown sinusoidal-like variation of the detection thresholds with improved detectability around January and July when the stratospheric winds are the strongest [e.g., Green and Bowers, 2010]. Here, the PE simulation results exhibit different patterns outlined below:

[30] 1. When downwind propagation occurs in both hemispheres, from November to March and May to September, any significant wind component in the stratosphere, such that $V_{\text{eff-ratio}} > 1$, generates signals of comparable attenuation. Thus, wind speed variations weakly influence the amount of propagated acoustic energy (attenuation varies within a range of ~ 5 dB). The difference between one, two, or three detecting stations is less pronounced than intuitively expected. When the average distance from an arbitrary source

location toward one to three detecting stations increases from ~ 2000 to ~ 2500 km, the attenuation controlled by β is only in the order of 6 dB.

[31] 2. Near the equinox periods, from March to May and September to November, the stratospheric winds reduce, yielding values of $V_{\text{eff-ratio}}$ close to 1. Near such value, the stratospheric duct becomes unstable. As a result of the represented daily meteorological variations in the ECMWF model, the acoustic energy could either return to the ground surface or escape to the thermosphere. Above 0.8 Hz, variations in attenuation may be as large as ~ 20 dB within periods of days.

[32] The attenuation is frequency-dependent due to absorption which increases with frequency [Sutherland and Bass, 2004]. Below 0.8 Hz, the 95% percentile of the attenuation calculated over the earth's surface is almost constant (between -60 and -80 dB with variations of ~ 5 dB throughout the year). At higher frequencies, larger seasonal variations are observed. During the seasonal transition between winter and summer, above 0.8 Hz and for three-station coverage, the attenuation varies within a range of ~ 30 dB. For one-station coverage, fluctuations reduce to ~ 10 dB.

4. Concluding Remarks

[33] A new attenuation relation has been derived from 9,120 PE numerical simulations using the wide-angle

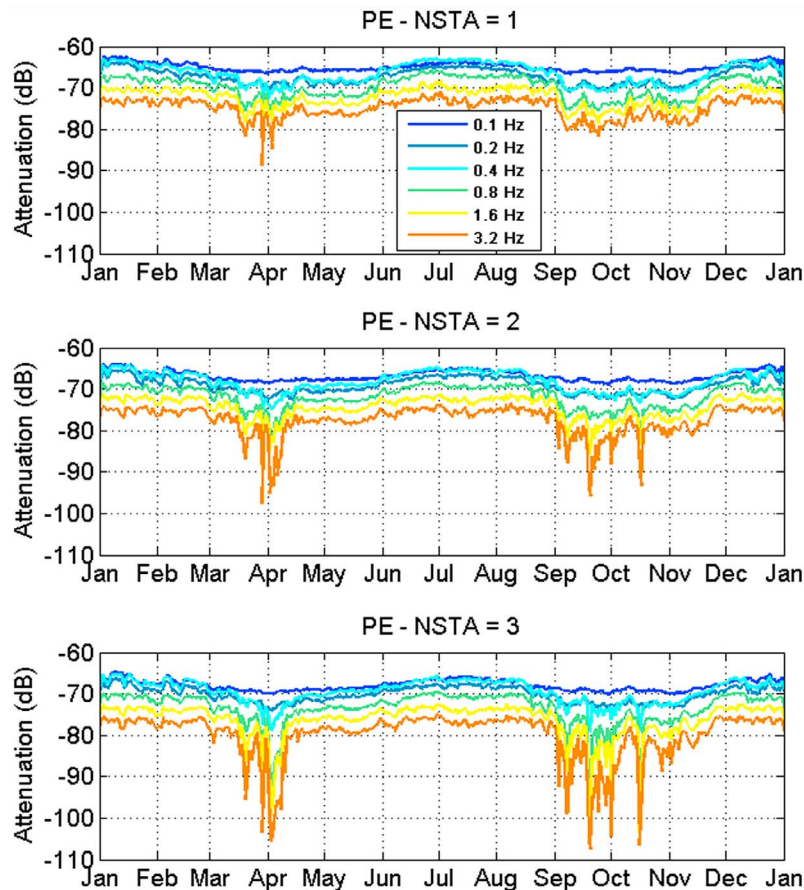


Figure 6. Yearly summary of the smallest signal attenuation at frequencies of 0.1, 0.2, 0.4, 0.8, 1.6 and 3.2 Hz with (top) one-, (middle) two- and (bottom) three-station coverage. The stratospheric wind components are derived from the ECMWF model. Curves indicate the 95% confidence interval calculated across the earth's surface.

parabolic equation method along with the integration of an accurate parameterization of the atmosphere. The relation incorporates the effects of the source frequency, the effective sound speed ratio in the stratosphere covering realistic down- and counter-wind scenarios, and fine-scale atmospheric structures. These simulations are aimed at increasing understanding of the effects these parameters have on long-range infrasound propagation. The proposed relation consists of two terms which quantify the attenuation in the shadow zone and in the geometrical acoustic duct region for both stratospheric and thermospheric returns. These two terms depend only on three frequency- and wind-dependent parameters picturing the main physical trends represented in the numerical simulations.

[34] The main difference between previous scaling relationships and our relation is the stratospheric wind effects on attenuation and a frequency-dependent examination accounting for corresponding anelastic attenuation in the atmosphere. While the LANL relation predicts exponential variation in signal amplitude with changing wind speed, our modeled attenuation follows an approximately binary variation with the effective sound speed ratio in the stratosphere. This step-like variation is more pronounced above 0.8 Hz; whereas at lower frequency the attenuation is less sensitive to the strength and direction of the prevailing stratospheric winds. This

relation provides improved explanations of recent multiyear global infrasound observations indicating good detection capability for downwind stations as long as $V_{\text{eff-ratio}}$ is larger than 1.

[35] The simulations of the performance of the IMS infrasound network highlight the influences of the combined effects of the source frequency and short time scale variations of stratospheric winds. Improved performance is predicted from December to March and May to September when downwind propagation occurs in both hemispheres. During the winter and summer seasons, the attenuation remains stable around -70 dB. During the equinox periods, zonal winds reduce and reverse, yielding above 1.6 Hz a ~ 30 dB increase of the attenuation. As a result of the meteorological fluctuations in the stratosphere, daily variations of the attenuation may be as large as ~ 20 dB above 0.8 Hz. According to these simulations, compared with previous detection capability studies, an improved performance of the IMS network is expected since efficient stratospheric ducting is modeled even under low wind conditions. This prediction is consistent with recent observations of calibration experiments showing multiple stations recording ~ 82 t of TNT explosion at distance of several thousands of kilometers [Gitterman *et al.*, 2009].

[36] Additional work is needed to validate the calculated attenuation maps using ground-truth events. Endeavors have been made to establish a comprehensive ground-truth database [e.g., O'Brien et al., 2007], well calibrated explosion experiments [e.g., Whitaker et al., 2003; Gitterman et al., 2009; Green et al., 2010; Gitterman and Hofstetter, 2011] as well as systematic location of repeating sources [e.g., Antier et al., 2007]. These databases, constantly updated, will provide a statistical approach for testing our relation.

[37] Further studies should also be pursued to model a more realistic picture of infrasound propagation. The numerical simulation approach used here provides a basis for such investigations. In particular, more accurate attenuation prediction could be obtained in the near-field by considering a frequency-dependent parameter δ . Meanwhile, in addition to the stratosphere, the vertical structure of the wind profiles could be adjusted in the troposphere and mesosphere to delineate more realistic atmospheric specifications. Such studies would better describe the infrasound propagation in the first hundreds of kilometers. The source altitude is another parameter which could be incorporated in the curve-fitting. One strong assumption made in this study is the range independence calculations. Such an approximation, generally applicable to distances of approximately 300–600 km, may introduce unrealistic simulation results at global ranges [Arrowsmith et al., 2007]. Numerical explorations with fully resolved, time- and range-dependent wave propagation techniques accounting for nonlinear propagation effects would provide more realistic results while still maintaining computational efficiency [e.g., McDonald and Kupperman, 1987]. We expect from such methods along with pertinent studies of ground-truth events clear indications if the assumption of a β being independent of the distance is justified or if a range-dependent β would be more appropriate.

[38] Finally, in order to calculate the detection capability of any infrasound network, additional developments are needed. By incorporating real ambient infrasound noise at the receivers [e.g., Bowman et al., 2005] which significantly limits the ability to detect and identify signals of interest, the minimum detectable source amplitude can be derived at single frequencies by applying equation (2). Following the same procedure, the minimum detectable source spectrum will be reconstructed in the frequency band of interest to detect explosions. By minimizing distance between the minimum detectable source spectrum and reference source spectrum of explosions [e.g., Glasstone and Dolan, 1977; Kinney and Graham, 1985], the explosive energy could then be derived in tons of TNT equivalent. Continuing such studies would help to further enhance network performance simulations and optimize future network design in order to monitor infrasonic sources of interest. This is an important step toward a successful monitoring regime for atmospheric or surface events and to act as an effective verification tool in the near future.

[39] **Acknowledgments.** The authors are grateful to Robin Matoza (Scripps Institution of Oceanography, University of California, San Diego) and D. Green (AWE Blacknest) for their interest in this study and helpful comments.

References

- Antier, K., A. Le Pichon, S. Vergnolle, C. Zielinski, and M. Lardy (2007), Multiyear validation of the NRL-G2S wind fields using infrasound from Yasur, *J. Geophys. Res.*, *112*, D23110, doi:10.1029/2007JD008462.
- Arrowsmith, S. J., D. P. Drob, M. A. H. Hedlin, and W. Edwards (2007), A joint seismic and acoustic study of the Washington State bolide: Observations and modeling, *J. Geophys. Res.*, *112*, D09304, doi:10.1029/2006JD008001.
- Balachandran, N. K., W. J. Donn, and G. Kaschak (1971), On the propagation of infrasound from rockets: Effects of winds, *J. Acoust. Soc. Am.*, *50*, 397–404, doi:10.1121/1.1912649.
- Barker, T. G. (1996), Xnice: A System for assessing network identification performance, *Maxwell Lab. Sci. Rep. PL-TR-96-2087*, Phillips Lab., La Jolla, Calif.
- Beranek, L. L. (1954), *Acoustics*, 481 pp., McGraw-Hill, New York.
- Blom, P., and R. Waxler (2010), What is learned about amplitude and waveform from geometric acoustics?, Abstract A41G-08 presented at 2010 Fall Meeting, San Francisco, Calif., 13–17 Dec.
- Bowman, J. R., G. E. Baker, and M. Bahavar (2005), Ambient infrasound noise, *Geophys. Res. Lett.*, *32*, L09803, doi:10.1029/2005GL022486.
- Brachet, N., D. Brown, R. Le Bras, P. Mialle, and J. Coyne (2010), Monitoring the Earth's atmosphere with the global IMS infrasound network, in *Infrasound Monitoring for Atmospheric Studies*, pp. 77–118, Springer, Dordrecht, Netherlands.
- Brown, D. J., C. N. Katz, R. Le Bras, M. P. Flanagan, J. Wang, and A. K. Gault (2002), Infrasonic signal detection and source location at the Prototype Data Centre, *Pure Appl. Geophys.*, *159*, 1081–1125, doi:10.1007/s00024-002-8674-2.
- Campus, P., and D. R. Christie (2010), Worldwide observations of infrasonic waves, in *Infrasound Monitoring for Atmospheric Studies*, pp. 195–234, Springer, Dordrecht, Netherlands.
- Ceranna, L., A. Le Pichon, D. N. Green, and P. Mialle (2009), The Buncefield explosion: A benchmark for infrasound analysis across central Europe, *Geophys. J. Int.*, *177*(2), 491–508, doi:10.1111/j.1365-246X.2008.03998.x.
- Christie, D. R., and P. Campus (2010), The IMS infrasound network: Design and establishment of infrasound stations, in *Infrasound Monitoring for Atmospheric Studies*, pp. 29–76, Springer, Dordrecht, Netherlands.
- Christie, D. R., V. Veloso, P. Campus, M. Bell, T. Hoffmann, A. Langlois, P. Martyshevich, E. Demirovic, and J. Carvalho (2001), Detection of atmospheric nuclear explosions: The infrasound component of the International Monitoring System, *Kerntechnik*, *66*, 96–101.
- Clauter, D. A., and R. R. Blandford (1997), Capability modelling of the proposed International Monitoring System 60-Station infrasonic network, paper presented at Infrasound Workshop for CTBT Monitoring, LANL, Santa Fe, N. M.
- Collins, D. (1993), A split-step Pade solution for parabolic equation method, *J. Acoust. Soc. Am.*, *93*, 1736–1742, doi:10.1121/1.406739.
- Drob, D. P., J. M. Picone, and M. Garcés (2003), Global morphology of infrasound propagation, *J. Geophys. Res.*, *108*(D21), 4680, doi:10.1029/2002JD003307.
- Drob, D. P., R. R. Meier, J. M. Picone, and M. A. Garcés (2010), Inversion of infrasound signals for passive atmospheric remote sensing, in *Infrasound Monitoring for Atmospheric Studies*, pp. 701–731, Springer, Dordrecht, Netherlands.
- Evers, L. G., L. Ceranna, H. W. Haak, A. Le Pichon, and R. W. Whitaker (2007), A seismo-acoustic analysis of the gas-pipeline explosion near Ghislenghien in Belgium, *Bull. Seismol. Soc. Am.*, *97*(2), 417–425, doi:10.1785/0120060061.
- Fritts, D. C., and M. C. Alexander (2003), Gravity wave dynamics and effects in the middle atmosphere, *Rev. Geophys.*, *41*(1), 1003, doi:10.1029/2001RG000106.
- Gainville, O., P. Blanc-Benon, E. Blanc, R. Roche, C. Millet, F. Le Piver, B. Despres, and P. F. Piserchia (2010), Misty picture: A unique experiment for the interpretation of the infrasound propagation from large explosive sources, in *Infrasound Monitoring for Atmospheric Studies*, pp. 575–598, Springer, Dordrecht, Netherlands.
- Garcés, M. A., R. A. Hansen, and K. G. Lindquist (1998), Traveltimes for infrasonic waves propagating in a stratified atmosphere, *Geophys. J. Int.*, *135*, 255–263, doi:10.1046/j.1365-246X.1998.00618.x.
- Gardner, C. S., C. A. Hostetler, and S. J. Franke (1993), Gravity wave models for the horizontal wave number spectra of atmospheric velocity and density fluctuations, *J. Geophys. Res.*, *98*(D1), 1035–1049, doi:10.1029/92JD02051.
- Gibson, R. G., D. P. Drob, and D. Broutman (2009), Advancement of techniques for modelling the effects of fine-scale atmospheric inhomogeneities on infrasound propagation, paper presented at 30th Monitoring Research Review: Ground-Based Nuclear Explosion Monitoring Technologies, Natl. Nuclear Security Admin., Portsmouth, Va.
- Gitterman, Y., and R. Hofstetter (2011), GT0 explosion sources for IMS infrasound calibration, winter 2011, *Geophys. Res. Abstr.*, *13*, EGU2011-1748.
- Gitterman, Y., M. A. Garcés, J. R. Bowman, D. Fee, H. G. Israelsson, R. Hofstetter, and V. I. Pinsky (2009), Near-source and far-regional

- infrasound observations for Sayarim test explosions, paper presented at 30th Monitoring Research Review: Ground-Based Nuclear Explosion Monitoring Technologies, MRR, Portsmouth, Va.
- Glasstone, S., and P. J. Dolan (1977), *The Effects of Nuclear Weapons*, 3rd ed., U.S. Gov. Printing Off., Washington, D. C., doi:10.2172/6852629.
- Green, D. N., and D. Bowers (2010), Estimating the detection capability of the International Monitoring System infrasound network, *J. Geophys. Res.*, *115*, D18116, doi:10.1029/2010JD014017.
- Green, D. N., A. Le Pichon, L. Ceranna, and L. Evers (2010), Ground truth events: Assessing the capability of infrasound networks using high resolution data analyses, in *Infrasound Monitoring for Atmospheric Studies*, pp. 599–625, Springer, Dordrecht, Netherlands.
- Green, D. N., J. Vergoz, R. Gibson, A. Le Pichon, and L. Ceranna (2011), Infrasound radiated by the Gerdec and Chelophechene explosions: Propagation along unexpected paths, *Geophys. J. Int.*, *185*, 890–910, doi:10.1111/j.1365-246X.2011.04975.x.
- Kinney, G., and K. Graham (1985), *Explosive Shocks in Air*, 2nd ed., Springer, New York.
- Kulichkov, S. N. (2010), On the prospects for acoustic sounding of the fine structure of the middle atmosphere, in *Infrasound Monitoring for Atmospheric Studies*, pp. 511–540, Springer, Dordrecht, Netherlands.
- Kulichkov, S. N., and G. A. Bush (2001), Rapid variations in infrasonic signals at long distances from one-type explosions, *Izv. Russ. Acad. Sci. Atmos. Oceanic Phys., Engl. Transl.*, *37*(3), 306–313.
- Kulichkov, S. N., G. A. Bush, and A. I. Svertilov (2002), New type of infrasonic arrivals in the geometric shadow region at long distances from explosions, *Izv. Russ. Acad. Sci. Atmos. Oceanic Phys., Engl. Transl.*, *38*(4), 397–402.
- Kulichkov, S. N., I. P. Chunchuzov, and O. I. Popov (2010), Simulating the influence of an atmospheric fine inhomogeneous structure on long-range propagation of pulsed acoustic signals, *Izv. Russ. Acad. Sci. Atmos. Oceanic Phys., Engl. Transl.*, *46*(1), 60–68, doi:10.1134/S0001433810010093.
- Le Pichon, A., E. Blanc, and D. Drob (2005), Probing high-altitude winds using infrasound, *J. Geophys. Res.*, *110*, D20104, doi:10.1029/2005JD006020.
- Le Pichon, A., J. Vergoz, E. Blanc, J. Guilbert, L. Ceranna, L. Evers, and N. Brachet (2009), Assessing the performance of the international monitoring system infrasound network: Geographical coverage and temporal variabilities, *J. Geophys. Res.*, *114*, D08112, doi:10.1029/2008JD010907.
- Le Pichon, A., J. Vergoz, Y. Cansi, L. Ceranna, and D. Drob (2010), Contribution of infrasound monitoring for atmospheric remote sensing, in *Infrasound Monitoring for Atmospheric Studies*, pp. 629–646, Springer, Dordrecht, Netherlands.
- Lingevitch, J. F., M. D. Collins, D. K. Dacol, D. P. Drob, J. C. W. Rogers, and W. L. Siegmann (2002), A wide-angle and high Mach number parabolic equation, *J. Acoust. Soc. Am.*, *111*, 729–734, doi:10.1121/1.1430683.
- Matoza, R. S., A. Le Pichon, J. Vergoz, P. Herry, J. M. Lalande, H. Lee, I. Y. Che, and A. Rybin (2011), Infrasonic observations of the June 2009 Sarychev Peak eruption, Kuril Islands: Implications for infrasonic monitoring of remote explosive volcanism, *J. Volcanol. Geotherm. Res.*, *200*, 35–48, doi:10.1016/j.jvolgeores.2010.11.022.
- McDonald, B. E., and W. A. Kupperman (1987), Time domain formulation for pulse propagation, *J. Acoust. Soc. Am.*, *81*, 1406–1417, doi:10.1121/1.394546.
- More, J. J. (1977), The Levenberg-Marquardt algorithm: Implementation and theory, in *Numerical Analysis, Lecture Notes Math.*, vol. 630, edited by G. A. Watson, pp. 105–116, Springer, New York.
- Norris, D., R. Gibson, and K. Bongiovanni (2010), Numerical methods to model infrasonic propagation through realistic specifications of the atmosphere, in *Infrasound Monitoring for Atmospheric Studies*, pp. 535–567, Springer, Dordrecht, Netherlands.
- O'Brien, M. S., D. P. Drob, and J. R. Bowman (2007), Improved infrasound event location, paper presented at 29th Seismic Research Review, Army Space and Missile Defense Command, Denver, Colo.
- Picone, J. M., A. E. Hedin, S. L. Coffey, J. Lean, D. P. Drob, H. Neal, D. J. Melendez-Alvira, R. R. Meier, and J. T. Mariska (1997), The Naval Research Laboratory program on empirical models of the neutral upper atmosphere, in *Aerodynamics, Adv. Astronaut. Sci.*, vol. 97, edited by F. R. Hoots et al., pp. 515–527, Am. Astronaut. Soc., San Diego, Calif.
- Sereno, T. J., S. R. Bratt, and G. Yee (1990), NetSim: A computer program for simulating detection and location capability of regional seismic networks, *Semi-Annual Tech. Rep. 90/1163*, 98 pp., SAIC, McLean, Va.
- Stevens, J. L., I. I. Divnov, D. A. Adams, J. R. Murphy, and V. N. Bourchik (2002), Constraints on infrasound scaling and attenuation relations from Soviet explosion data, *Pure Appl. Geophys.*, *159*, 1045–1062, doi:10.1007/s00024-002-8672-4.
- Sutherland, L. C., and H. E. Bass (2004), Atmospheric absorption in the atmosphere up to 160 km, *J. Acoust. Soc. Am.*, *115*(3), 1012–1032, doi:10.1121/1.1631937.
- Trost, L. (1997), High altitude wind effects on infrasound network performance, paper presented at Infrasound Workshop for CTBT Monitoring, Off. of Defense Programs, DOE, Santa Fe, N. M.
- U.S. Committee on Extension to the Standard Atmosphere (1976), U.S. Standard Atmosphere 1976, *ADA-035-6000*, NTIS, Springfield, Va.
- Whitaker, R. W. (1995), Infrasonic monitoring, paper presented at 17th Annual Seismic Research Symposium, LANL, Scottsdale, Ariz.
- Whitaker, R. W., and J. P. Mutschlechner (2008), A comparison of infrasound signals refracted from stratospheric and thermospheric altitudes, *J. Geophys. Res.*, *113*, D08117, doi:10.1029/2007JD008852.
- Whitaker, R. W., T. D. Sandoval, and J. P. Mutschlechner (2003), Recent infrasound analysis, paper presented at 25th Annual Seismic Research Symposium, LANL, Tucson, Ariz.

L. Ceranna, BGR, B4.3, D-30655 Hannover, Germany.

A. Le Pichon and J. Vergoz, CEA/DAM/DIF, F-91297 Arpajon CEDEX, France. (alexis.le-pichon@cea.fr)